Title	Rational-design of polyaniline cathode using proton doping strategy by graphene oxide for enhanced aqueous zinc-ion batteries
Author(s)	Wencheng Du, Jinfei Xiao, Hongbo Geng, Yang Yang, Yufei Zhang, Edison Huixiang Ang, Minghui Ye and Cheng Chao Li
Source	*Journal of Power Sources*, *450*: Article 227716
Published by	Elsevier

Rational-Design of Polyaniline Cathode using Proton Doping Strategy by Graphene Oxide for Enhanced Aqueous Zinc-Ion Batteries

Wencheng Du,[a] *Jinfei Xiao,*[a] *Hongbo Geng,*[a] *Yang Yang,*[a] *Yufei Zhang,*[a] *Edison Huixiang Ang,*[b] *Minghui Ye*[a] *and Cheng Chao Li**[a]

[a] School of Chemical Engineering and Light Industry, Guangdong University of Technology, Guangzhou 510006, China

E-mail: licc@gdut.edu.cn

[b] Natural Sciences and Science Education, National Institute of Education, Nanyang Technological University, Singapore 637616, Singapore.

Abstract: Aqueous zinc-ion batteries (ZIBs) have been of excellent interest in latest years due to their friendly environment and easy preparation. One vital barrier to the production of high-performance ZIBs is the development of appropriate cathode materials. Polyaniline (PANI) is very promising, particularly due to its excellent

conductivity and easy preparation, among varied cathode materials. However, deprotonation of PANI is a key problem greatly deteriorating capacity and cycling stability of PANI cathode. In this study, we discover that graphene oxide (GO) can fix the problem effectively as the wealthy functional GO oxygen groups can provide a local proton reservoir that increases PANI protonation. As a result, the GO composited PANI electrodes show significantly improved zinc-ion storage performance than pure carbon composited PANI cathodes. Specifically, the battery performances in terms of capacity (233 mA h g^{-1}) and rate performance (100 mA h g^{-1} under 5 A g^{-1}) are enhanced significantly after introducing GO into PANI cathode. In addition, a flexible PANI-based ZIB devices can be easily fabricated owing to the excellent film-forming property of GO. This work offers a new insight for improving PANI cathode materials by carbon chemistry.

Keywords: polyaniline, graphene oxide, doping, aqueous zinc-ion batteries, flexible device

1. Introduction

Rechargeable batteries especially lithium-ion batteries based on organic electrolytes have attracted great attention because of their high capacity and energy density. However, the safety and resource scarcity greatly restricted their widely application in the large-scale application. So, the elevated safety and environmental compatibility of

the secondary metal-ion battery in latest years has attracted a lot of attention and made their applications easier in big power storage devices. In recent years, numerous rechargeable aqueous batteries based on different metal ions including lithium, sodium, potassium, magnesium, aluminum and zinc have been developed.[1–3] Among them, aqueous zinc-ion batteries (ZIBs) have become one promising energy system because of numerous merits of zinc metal mainly including high theoretical capacity (819 mA h g^{-1}), excellent compatibility with water, abundant reserves and low cost.[4–8] So, aqueous ZIBs possess great promise for practical applications. Factually, the study of ZIBs is still in its infancy and the development of high capacity cathode materials is one of the most pressing challenges. Although a number of cathode materials, metal oxide included, [9–13] organic small molecules/polymers[14–20] have been developed, the battery performance of these materials needs to be further improved. Polyaniline (PANI) has been shown to be an excellent cathode material for zinc storage, as a commonly used polymer based electrode material, and PANI offers significant benefits in terms of easy preparing, good conductivity and versatile processing capability. However, PANI cathode materials show low capacity typically below 200 mA h g^{-1}. [19, 21–26] One critical reason for this undesirable performance is deactivation of PANI caused by deprotonation of PANI in low acidic electrolytes such as $ZnSO_4$ or $Zn(CF_3SO_3)_2$ which are the common electrolytes in ZIBs. [27–31] Some techniques have been created based on the building of a local proton reservoir to help fix this issue and enhance the efficiency of the PANI cathode during electric procedures. For example, self-doping strategy based on introducing sulfonic acid

group by chemically modify PANI molecular backbone was proposed, and the sulfonic acid group modified PANI show enhanced long cycle stability.[19] Another method based on compositing PANI with other polymer containing sulfonic acid group such as PEDOT:PSS was also reported, and obvious enhanced capacity as well as enhanced capacity and cyclability was realized. [20] Although these approaches can improve ZIB's performance, its capacity needs further improvement and these approaches employ complicated, multistep chemical modifications or expensive PEDOT: PSS reagents that cannot be practically used. From a practical point of view, simpler and more efficient strategy is needed for improving battery performance of PANI.

In this respect, we report an effective and fairly easy technique for clearly improving the PANI's battery efficiency by using graphene oxide (GO) as effective doping species. The GO doped PANI can deliver very high reversible discharge capacity up to 225 mA h g^{-1}. Rate performance and long cycle stability of the GO doped PANI was also improved obviously. The mechanism of improved zinc storage benefited from the proton doping impact of GO because of its wealthy oxygen functional groups such as hydroxyl and carboxyl groups. In addition, GO sheets promote the construction of paper-like PANI cathode which can be used easily to manufacture flexible ZIB devices.

2. Experimental

Preparation of PANI/DMSO dispersion. PANI was synthesized according to a rapid mixing method as reported in the literature. [32] Briefly, 1.0 mL of aniline (Standard

for GC, ≥99.9%) was dissolved in 10.0 mL of 1M HCl solution, then 10.0 mL of 0.5 M $NH_4S_2O_8$ was quickly added into the acid solution in a beaker. The mixture was left overnight. The as-obtained PANI was washed by 1M HCl solution, pure water and ethanol respectively. Finally, the purified PANI was dissolved in DMSO, forming PANI/DMSO dispersion with concentration of 6.20 mg mL^{-1}.

Preparation of GO/DMSO dispersion. GO is prepared by the ethanol purified method.[33, 34] Typically, the freshly prepared graphite oxide obtained by the modified Hummers' method was purified by using 1M HCl to remove residual metal ion and then using absolute ethanol to wash again to remove residual HCl. The purified graphite oxide was air dried to remove additional ethanol until the ethanol residue was less than 30 wt%. The ethanol wetted graphite oxide was added in DMSO, and let it spontaneously swelling first. Finally, short-time (10-20 min) sonication was performed to get completely exfoliated GO sheets dispersed in DMSO, forming GO/DMSO dispersion with concentration of 3.00 mg mL^{-1}.

Preparation of CNT/DMSO dispersion. Homogeneous CNT dispersion was obtained by sonicating multiwalled CNT (40−60 nm in diameter and 5−15 μm in length, Shenzhen Nanotech Port Co. Ltd.) in DMSO with the assistance of sodium citrate as reported.[35] Finally, the concentration of the as-obtained GO/DMSO dispersion is set as 2.00 mg mL^{-1}.

Preparation of series of PANI-based film electrodes. For fabricating PANI/CNT film, 2.00 mL of PANI/DMSO and 2.50 mL of CNT/DMSO were mixed and then vacuum

filtered through a nylon filter membrane (0.45 μm pore size). When no free dispersion was left on the filtrate film, 4 mL of 1M HCl(aq) and 20 mL of water was added in sequence to vacuum filter continually. The as-obtained PANI/CNT film attached on the nylon filter membrane substrate was punched into electrode slices with diameter of 12 mm, and the electrode slices were directly use to assembly coin-type ZIBs. The mass loading of PANI in each electrode slice is 1.00 mg.

For fabricating PANI-GO/CNT film, 2.00 mL of PANI/DMSO, 2.50 mL of CNT/DMSO and 1.00 mL of GO/DMSO were mixed and then vacuum filtered similar with the case for the PANI/CNT film. The GO content is optimized to 20 wt%.

Assembly of the coin-type ZIB devices. The electrochemical properties of the PANI-based electrode slices were evaluated by using CR2032 coin cells with zinc as an anode and Whatman film as a separator. The coin cells were assembled under natural ambient conditions. 120 μL of 2.5 M zinc trifluoromethanesulfonate ($Zn(CF_3SO_3)_2$) in water with 5 vol% diethyl ether served as the electrolyte. The cells were galvanostatically charged and discharged between 0.5 and 1.6 V versus Zn^{2+}/Zn on a NEWARE battery tester. The cyclic voltammetry (CV) was conducted on Gamry electrochemical station. The capacity of the samples was calculated based on the weight of PANI.

Assembly of the flexible ZIB devices. The flexible ZIB with a layer-cake model was assembled by free-standing PANI-GO/CNT cathode, Zn foil anode, PVA-based gel electrolyte and graphite paper collector. PVA-based hydrogel electrolyte was obtained

by dissolving 1.5 g of PVA in 4.0 mL of water, and then adding 5.0 mL of 2.5 M $Zn(CF_3SO_3)_2$ electrolyte as mentioned above. For the fabrication of flexible battery, one-piece graphite paper was put on a PVC plate; then the PANI-GO/CNT film, filter paper soaked with PVA-based gel electrolyte, a Zn foil, another graphite paper and another PVC plate were placed on the top in sequence. Finally, the battery was sealed with epoxy glue before testing.

Characterizations. Scanning electron microscopy (SEM) (S4800, Hitachi, operating at 10 kV), and energy-dispersive X-ray spectroscopy (EDX) (S4800, Hitachi, operating at 20 kV) were performed. Transmission electron microscopy (TEM) (JEM-2100F, operating at 200 kV) were also conducted. XPS spectra were recorded on an ESCALAB 250 photoelectron spectrometer (ThermoFisher Scientific) with Al Kα (1486.6 eV) as the X-ray source set at 150 W and a pass energy of 30 eV for high resolution scan. Attenuated total reflectance-Fourier transform infrared spectroscopy (ATR-FTIR) spectra were recorded on a Fourier transform infrared spectrometer (Bruker Vertex V70). Raman characterization was carried out on a LabRAM HR800 spectrometer (Horiba) using a 633 nm laser. Zeta potentials were determined by using a Surpass zeta potential analyzer (Anton Paar, Austria).

3. Results and discussions

Solution-based compositing technique is a very efficient route to get highly homogeneous composite materials. Figure 1a shows the scheme of preparing GO composited PANI electrode materials based on excellent dispersibility of GO and

PANI in certain solvent. In our experiment, we found the pure PANI and PANI-GO electrodes have very large charge transfer resistance and results in poor electrochemical performances (Figure S1). So, conductive additive is needed for obtaining ideal battery performance. CNT was used as conductive additive and it is effective that CNT greatly reduce the charge transfer resistance of the final composites (Figure S1). DMSO act as co-solvent, because these components (PANI, GO and CNT) can well dispersed in DMSO.[33–36] The as-obtained stable colloidal dispersions of these components can be directly blended and then vacuum filtered to get composite film denoted as PANI-GO/CNT which can be directly punched into electrode slices (Figure S2). The excellent dispersion of PANI、GO and CNT in DMSO is demonstrated by TEM characterizations (Figure 1b-d, Figure S3). PANI shows nanorod morphology with the width of around 50 nm. While GO and CNT components show typical nanosheet and nanowire morphologies respectively. All of these components are dispersed well without aggregation. The great dispersion of the three components ensures that the composites are finally uniform. Figure 1e-g show the SEM image and corresponding energy dispersive X-ray spectroscopy (EDS) mapping of the GO-PANI/CNT film. The EDS mapping of nitrogen and oxygen elements are rather uniformly distributed, implying the homogenous composting of the GO and PANI components.

The compositing between GO and PANI can create new intermolecular interactions, such as hydrogen bonding, van der Waals' forces and electrostatic interactions, because of the many oxygen-containing functional groups in the GO sheets and

nitrogen functional groups in the PANI backbone. The interaction between GO and PANI can be reflected by FT-IR spectra (Figure 2a, b). It should be mentioned that these peaks come from the GO and PANI components rather than CNT because the CNT is without any chemical modifications and thus show almost no peaks (Figure S4) compared with GO and PANI components. In the PANI-GO/CNT composite, the characteristic peaks of GO located at 3239 (ν_{O-H}), 1727 ($\nu_{C=O}$), 1408 (δ_{O-H}), 1224 (ν_{C-OH}), 1066 cm^{-1} (ν_{C-O}) and PANI located at 1589 ($\nu_{C=N}$), 1306 cm^{-1} (ν_{C-N}) become broaden and weak, suggesting the existence of non-covalent bond associated structure caused by hydrogen bonding and so on. [37–39] More importantly, the PANI-GO interactions lead to effective PANI proton acid doping, which is essential to improve PANI cathode's electrochemical performances. Raman characterization demonstrated the doping phenomenon (Figure S5). The Raman spectra of CNT and GO display two typical peaks of carbon nanomaterials at 1334 (1329 for GO) and 1586 (1596 for GO) cm^{-1} that correspond to the D and G bands, respectively.[40] The G band is ascribed to the vibration of sp^2-hybridized carbon and the D band is related with defect structure caused by sp^3-hybridized carbon. For PANI, typical peaks located at 418, 528, 815, 1168, 1228, 1339, 1465, and 1601 cm^{-1} were observed. [37, 41] Among these peaks, the intensity of doped C-$N^{\bullet+}$ stretching signal located at 1339 cm^{-1} is significant increased after composting PANI with GO component. This should be mainly ascribed to the doping of oxygen functional groups such as carboxyl acid of GO to PANI backbone.[37] The proton doping effect was demonstrated by XPS analysis (Figure 2c-e). Typically, four types of N including non-protonated imine –N= (398.9 eV),

non-protonated amine –NH– (399.5 eV), protonated amine –NH^+– (400.6 eV) and protonated imine –NH^+= (402.0 eV) can be existed in PANI.[19, 20] Proton doping can increase the ratio of protonated N. According the N1s results, the protonated N (–NH^+= and –NH^+–) in PANI-GO/CNT is 61%, which is much higher than that of PANI/CNT with only 38%. The proton doping effect stem from the rich oxygen-containing functional groups such as carboxyl and hydroxyl which can act as proton reservoir providing a steady supply of active proton.[42, 43] The local acid doping is vital for achieving enhanced electrochemical performance of PANI cathode.

A typical coin-type aqueous zinc cells were constructed based on PANI/CNT and PANI-GO/CNT as electrodes with equal mass loading of PANI in order to systematically assess the electrochemical performance of the PANI with and without GO doping. Figure 3 show the significantly improved zinc storage performances of GO doped PANI cathode. Figure 3a and b present the discharge and charge profiles of PANI-GO/CNT and PANI/CNT respectively. The average discharge voltage of the two PANI electrodes with or without GO is both around 1.1 V, while the GO doped PANI show higher discharge voltage than pure PANI cathode. This can be attributed to the higher oxidative state of PANI due to stronger proton doping effect. The PANI-GO/CNT nanocomposite can deliver a discharge capacity as high as 247 mA h g^{-1} for the first cycle and 233 mA h g^{-1} for the second cycle. In contrast, the PANI/CNT shows smaller capacity with 102 mA h g^{-1} and 175 mA h g^{-1} for the initial and second cycle respectively. The rate capability of the PANI-GO/CNT cathode was also investigated (Figure 3c, d and Figure S6). The GO doped PANI

displays a good rate performance with reversible specific capacities of 233, 202, 186, 166, 127 and 100 mA h g^{-1} at 0.1, 0.3, 0.5, 1.0, 3.0, and 5.0 A g^{-1}, respectively. The battery performances are obviously superior to GO-free PANI case, suggesting the GO is vital for improving the battery performances. The PANI component contributes mainly to the capacity, because GO/CNT is an insignificant capacity element (Figure S7). Compared with other PANI cathodes only using conductive carbon materials as composite components such as graphene,[25] CNT,[26] carbon felt[23] and carbon fiber[21], the GO composited PANI/CNT show higher reversible capacity and better rate performances (Table 1). So, this suggests that introducing carbon materials with both conductivity and acidic groups will be better strategy for enhancing zinc storage performance of PANI cathodes. Figure 3e shows the cycling performance of PANI-GO/CNT cathode at 3 A g^{-1}. The specific capacity of the PANI-GO/CNT cathode can maintain approximately 100 mA h g^{-1} after 2500 cycles, suggesting the good long-term cycling stability.

Cyclic voltammetry curves of PANI electrodes with and without GO doping were evaluated with distinct sweeping rates from 0.05 to 0.6 mV s^{-1}, in order to comprehend the mechanism for enhanced response kinetics for the GO doped PANI. Figure 4a, b shows a main pair of peaks in cathodic and anodic processes for both PANI-GO/CNT and PANI/CNT. Obviously, the GO doped PANI has sharper peaks as well as larger current density response than PANI cathode without GO doping. Moreover, the polarization is much smaller for GO doped PANI as the stepwise increase of the scan rate from 0.05 to 0.6 mV s^{-1} between 0.5-1.6 V (vs. Zn^{2+}/Zn).

More redox peaks presented for PANI-GO/CNT case which are mainly from different N groups derived from GO doping effect toward PANI. Three cathodic peaks are detected at 1.20 V, 0.75 V and 0.65 V, which is ascribed to the reduction of N components with the oxidized state including –NH^+=, –NH^+– and –N=.[19, 20] The two anodic peak at 1.15 V and 1.4 V should be associated with the multi-step oxidation of non-protonated nitrogen of –NH–.[19, 20] The electrochemical processes of PANI-GO/CNT is superior than the PANI/CNT which exhibits sluggish redox peaks. These facts show, in fact, that GO improved PANI electrode material electrochemical kinetics, and is in agreement with the rapid rate capabilities and higher capacity observed. Furthermore, the relationship between the peak currents (i) and scan rates (v) in form of $i = av^b$ can be used to analyze the electrochemical details of an ion storage reaction.[44] It is known that the b-value is a key parameter for indicating diffusion-controlled process (when b = 0.5) or surface capacitance-dominated behavior (when b = 1). As shown in Figure 4c, the b-values determined by the slopes of the four redox peaks are 0.71, 0.68, 0.99 and 0.93, respectively, suggesting that the electrochemical reactions are both mainly dominated by the pseudocapacitive behavior. It is clear that the GO doping effect greatly increase electrochemical activity of PANI and thus result in larger surface-dominated pseudocapacitance.

The enhanced electrochemical activity is essentially attributed to the specific molecular structure of GO. It has been reported that -SO_3H group covalently modified in PANI backbone can be ionized in $ZnSO_4$ electrolyte (pH =4.2) and form -SO_3^-

groups. [19] The $-SO_3^-$ groups act as self-dopants and internal proton reservoirs to ensure high local H^+ concentration and facilitate the redox process of PANI cathode in the weakly acidic electrolyte. Similar with the $-SO_3H$ group, oxygen functional groups such as -COOH in GO can also be ionized in the weakly acidic $Zn(CF_3SO_3)_2$ electrolyte (pH=4). This fact is confirmed by measuring zeta potential of solid surfaces (here is GO film). The zeta potential of GO film was measured to be – 36.39 mV in the aqueous electrolyte with the same pH value of 4 with the $Zn(CF_3SO_3)_2$ electrolyte (Figure S8). So the resulting $-COO^-$ will have the same function with reported $-SO_3^-$ groups. So, the oxygen functional group in GO is vital for the effective enhancement towards electrochemical performances of PANI. This can be confirmed by the phenomena that the enhancement will be disappeared when the oxygen functional groups in GO is largely removed by reducing agent, forming rGO counterpart (Figure 4d-f). It can be seen that the PANI-rGO/CNT show similar battery performance with PANI/CNT, which can only deliver reversible discharge capacity much lower than 200 mA h g^{-1}. Similar with the case in PANI/CNT, the rate performance of PANI-rGO/CNT is much lower than the original GO doped PANI electrode (i.e. PANI-GO/CNT). So, the critical role of oxygen functional groups in GO is further demonstrated from the opposite angle by observing the deteriorated battery performance of PANI-rGO/CNT electrode in which oxygen functional groups are removed. This deteriorated battery performance is that the rGO can only serve as conductive additive, it cannot produce an effective proton acid doping effect. So, good

conductivity and local proton reservoir are both essential factors determining the ultimate performance of PANI cathode.

GO macromolecule not only provides the local proton environment, but also makes 2D film structure easy to form. The PANI-GO/CNT, achieved as such, can automatically peel off from the nylon microfiltration membrane substrate, thanks to the outstanding film-forming characteristics of two-dimensional GO sheets. The free-standing PANI-GO/CNT film show excellent flexibility as shown in Figure 5a. After bending and even folding, the integrity of the PANI-GO/CNT film can be maintained. Such astonishing flexible characteristic of PANI-GO/CNT is very useful to manufacture versatile ZIB. For example, the flexible ZIB was manufactured with PANI-GO/CNT film assembled with gel electrolyte and Zn anode and the device was finally encapsulated between a transparent polyvinyl chloride (PVC) platform (Figure 5b, c). The as-obtained ZIB device show excellent flexibility, and electrochemical characterizations show the flexible ZIB can still give high capacity and rate performances which can be comparable with typical coin-type cell. The flexible ZIB device displays high discharge capacity up to 239 mA h g^{-1} for the first cycle and 199 mA h g^{-1} for the second cycle, and good rate performances with reversible specific capacities of 180, 165, 155, 143, 120 and 108 mA h g^{-1} at 0.1, 0.3, 0.5, 1.0, 3.0, and 5.0 A g^{-1}, respectively(Figure 5d). The capacity for the flexible ZIB devices is not well recovered which may be caused by the gel-based electrolyte which was partly consumed during cycling. The versatile ZIB can offer nearly the same battery performance under bending conditions (Figure 5e, f). This indicates the high

flexibility and performance of batteries that will help to develop a flexible power device for future flexible electronics, such as a bendable cellphone, etc.

Conclusions

In this work, we have shown a rather easy approach to enhance the zinc storage efficiency of PANI considerably through the introduction of GO sheets as a particular dopant. The GO component provides local proton reservoir and efficiently protonate PANI because of numerous of oxygen-containing functional groups. Therefore, during the charging/discharging processes, PANI undesirable deprotonation is significantly weakened. So, the battery performance of PANI is significantly improved in terms of high capacity above 200 mA h g^{-1} and show excellent rate performance, which is superior than other carbon-based materials composited PANI. These results show that GO is a key carbon material to enhance PANI electrochemical activity, because GO can deliver proton which is more relevant for the improvement of electrochemical results. The GO composted PANI can also easily form stand-alone film electrode that is easily used in the production and development of versatile high-level ZIBs.

Acknowledgements

This work was financially supported by the National Natural Science Foundation of China (Grant No. 51771058, Grant No. 51801030), Natural Science Foundation of Guangdong Providence (Grant No. 2018A030310571), One-hundred Young Talents (Class A) of Guangdong University of Technology (Grant No. 220413198), Pearl

River Talent Program of Guangdong Province (2017GC010030), Guangdong Province Universities and Colleges Pearl River Scholar Funded Scheme.

References

[1] H. Kim, J. Hong, K. Y. Park, H. Kim, S. W. Kim, K. Kang, Chem. Rev. 1142 (2014) 11788–11827.

[2] N. Alias, A. A. Mohamad, J. Power Sources 274 (2015) 237–251.

[3] Y. Wang, J. Yi, Y. Xia, Adv. Energy Mater. 2 (2012) 830–840.

[4] A. Konarov, N. Voronina, J. H. Jo, Z. Bakenov, Y. Sun, S. Myung, ACS Energy Lett. 3 (2018) 2620–2640.

[5] G. Fang, J. Zhou, A. Pan, S. Liang, ACS Energy Lett. 3 (2018) 2480–2501.

[6] C. Xu, B. Li, H. Du, F. Kang, Angew. Chem. Int. Ed. 124 (2012) 933–935.

[7] H. Pan, Y. Shao, P. Yan, Y. Cheng, K. S. Han, Z. Nie, C. Wang, J. Yang, X. Li, P. Bhattacharya, K. T. Mueller, J. Liu, Nat. Energy 1 (2016) 16039.

[8] D. Kundu, B. D. Adams, V.Duffort, S. H.Vajargah, L.F. Nazar, Nat. Energy 1 (2016) 16119.

[9] N. Zhang, F. Cheng, J. Liu, L. Wang, X. Long, X. Liu, F. Li, J. Chen, Nat. Commun. 8 (2017) 405.

[10] B. Wu, G. Zhang, M. Yan, T. Xiong, P. He, L. He, X. Xu, L. Mai, Small 14 (2018) 1703850.

[11] J. Hao, J. Mou, J. Zhang, L. Dong, W. Liu, C. Xu, F. Kang, Electrochim. Acta. 259 (2018) 170–178.

[12] P. Senguttuvan, S. D. Han, S. Kim, A. L. Lipson, S. Tepavcevic, T. T. Fister, I. D. Bloom, A. K. Burrell, C. S. Johnson, Adv. Energy Mater. 6 (2016) 1600826.

[13] J. Zhou, L. Shan, Z. Wu, X. Guo, G. Fang, S. Liang, Chem. Commun. 54 (2018) 4457–4460.

[14] D. Kundu, P. Oberholzer, C. Glaros, A. Bouzid, E. Tervoort, A. Pasquarello, M. Niederberger, Chem. Mater. 30 (2018) 3874–3881.

[15] Y. Lu, Q. Zhang, L. Li, Z. Niu, J. Chen, Chem 4 (2018) 2786–2813.

[16] Q. Zhao, W. Huang, Z. Luo, L. Liu, Y. Lu, Y. Li, L. Li, J. Hu, H. Ma, J. Chen, Sci. Adv. 4 (2018) eaao1761.

[17] K. Koshika, N. Sano, K. Oyaizu, H. Nishide, Macromol. Chem. Phys. 210 (2009) 1989–1995.

[18] C. Chen, X. Hong, A. Chen, T. Xu, L. Lu, S. Lin, Y. Gao, Electrochim. Acta 190 (2016) 240–247.

[19] H. Shi, Yi. Ye, K. Liu, Y. Song, X. Sun, Angew. Chem. Int. Ed. 130 (2018) 16597–16601.

[20] Y. Liu, L. Xie, W. Zhang, Z.Dai, W. Wei, S. Luo, X. Chen, W. Chen, F. Rao, L. Wang, Y. Huang, ACS Appl. Mater. Interfaces 11 (2019) 30943–30952.

[21] C. Kim, B. Y. Ahn, T. Wei, Y. Jo, S. Jeong, Y. Choi, I. Kim, J. A. Lewis, ACS Nano 12 (2018) 11838–11846.

[22] Y. Ma, X. X., R. Lv, B. Na, J. Ouyang, H. Liu, ACS Sustainable Chem. Eng. 6 (2018), 8697–8703.

[23] F. Wan, L. Zhang, X. Wang, S. Bi, Z. Niu, J. Chen, Adv. Funct. Mater. 28 (2018) 1804975.

[24] S. Huang, F. Wan, S. Bi, J. Zhu, Z. Niu, J. Chen, Angew. Chem. 131 (2019) 4357–4361.

[25] J. Han, K. Wang, W. Liu, C. Li, X. Sun, X. Zhang, Y. An, S. Yi and Y. Ma, Nanoscale 10 (2018) 13083–13091.

[26] A. Guerfi, J. Trottier, I. Boyano, I. De Meatza, J.A. Blazquez, S. Brewer, K.S. Ryder, A. Vijh, K. Zaghib, J. Power Sources 248 (2014) 1099–1104.

[27] F. Trinidad, M. C. Mentemayor, M. Fatás, J. Electrochem. Soc. 138 (1991) 3186–3189.

[28] H. Karami, M. F. Mousavi, M. Shamsipur, J. Power Sources 117 (2003) 255–259.

[29] J. Yue, Z. H. Wang, K. R. Cromack, A. J. Epstein, A. G. MacDiarmid, J. Am. Chem. Soc. 113 (1991) 2665–2671.

[30] A. A.Karyakin, A. K. Strakhova, A. K. Yatsimirsky, J. Electroanal. Chem. 371 (1994) 259–265.

[31] M. S. Rahmanifar, M. F. Mousavi, M. Shamsipur, J. Power Sources 110 (2002) 229–232.

[32] J. Qiang, Z. Yu, H. Wu, D.Yun, Synthetic Metals, 158 (2008), 544–547.

[33] W. Du, M. Wu, M. Zhang, G. Xu, T. Gao, L. Qian, X. Yu, F. Chi, C. Li, G. Shi, Chem. Commun. 53 (2017) 11005–11007.

[34] W. Du, M. Wu, M. Zhang, G. Xu, T. Gao, L. Qian, X. Yu, F. Chi, C. Li, G. Shi, Carbon 129 (2018) 15–20.

[35] W. Du, S. Qi, Y. Zhu, P. Sun, L. Zhu, X. Jiang, Chem. Eng. J. 262 (2015) 658–664.

[36] W. Du, H. Geng, Y. Yang, Y. Zhang, X. Rui, C. Li, J. Power Sources 43 (2019) 226899.

[37] H. Wang, Q. Hao, X. Yang, L. Lu, X. Wang, ACS Appl. Mater. Interfaces 2 (2010) 821–828.

[38] H. Wang, Q. Hao, X. Yang, L. Lu, X. Wang, Electrochem. Commun. 11 (2009) 1158–1161.

[39] J. Xu, K. Wang, S. Zu, B. Han, Z. Wei, ACS Nano 4 (2010) 5019–5026.

[40] K.N. Kudin, B. Ozbas, H. C. Schniepp, R. K. Prud'homme, I. A. Aksay, R. Car, Nano Lett. 8 (2008) 36–41.

[41] Z. Wei, M. Wan, T. Lin, L. Dai, Adv. Mater. 15 (2003) 136–139.

[42] A. Dimiev, D. V. Kosynkin, L. B. Alemany, P. Chaguine, J. M. Tour, J. Am. Chem. Soc. 134 (2012) 2815–2822.

[43] A. M. Dimiev, L. B. Alemany, J. M. Tour, ACS Nano 7 (2013) 576–588.

[44] J. B. Cook, H.-S. Kim, T. C. Lin, C.-H. Lai, B. Dunn, S.H. Tolbert, Adv. Energy Mater. 7 (2017) 1601283.

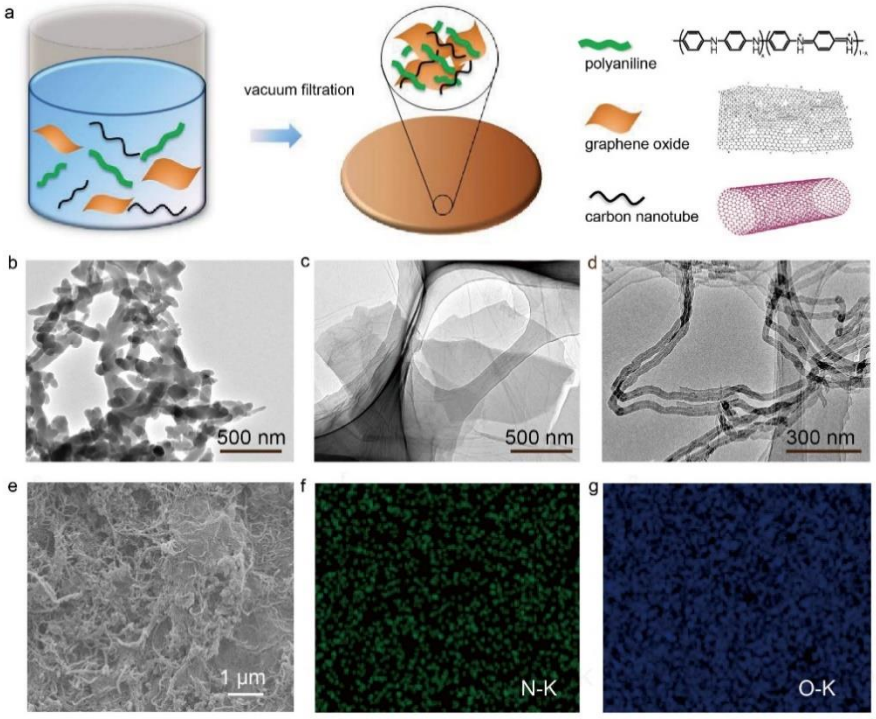

Figure 1. (a) Scheme of preparing PANI-GO/CNT composite film based on vacuum filtration of homogeneous dispersion of PANI, GO and CNT in DMSO solvent. (b-e) TEM images of the dispersed PANI、GO and CNT. (e) SEM of the as-obtained PANI-GO/CNT composite after vacuum filtration, and (f, g) corresponding EDS mapping of the nitrogen (N) and oxygen (O), indicating the uniform distribution of GO and PANI in the PANI-GO/CNT composite.

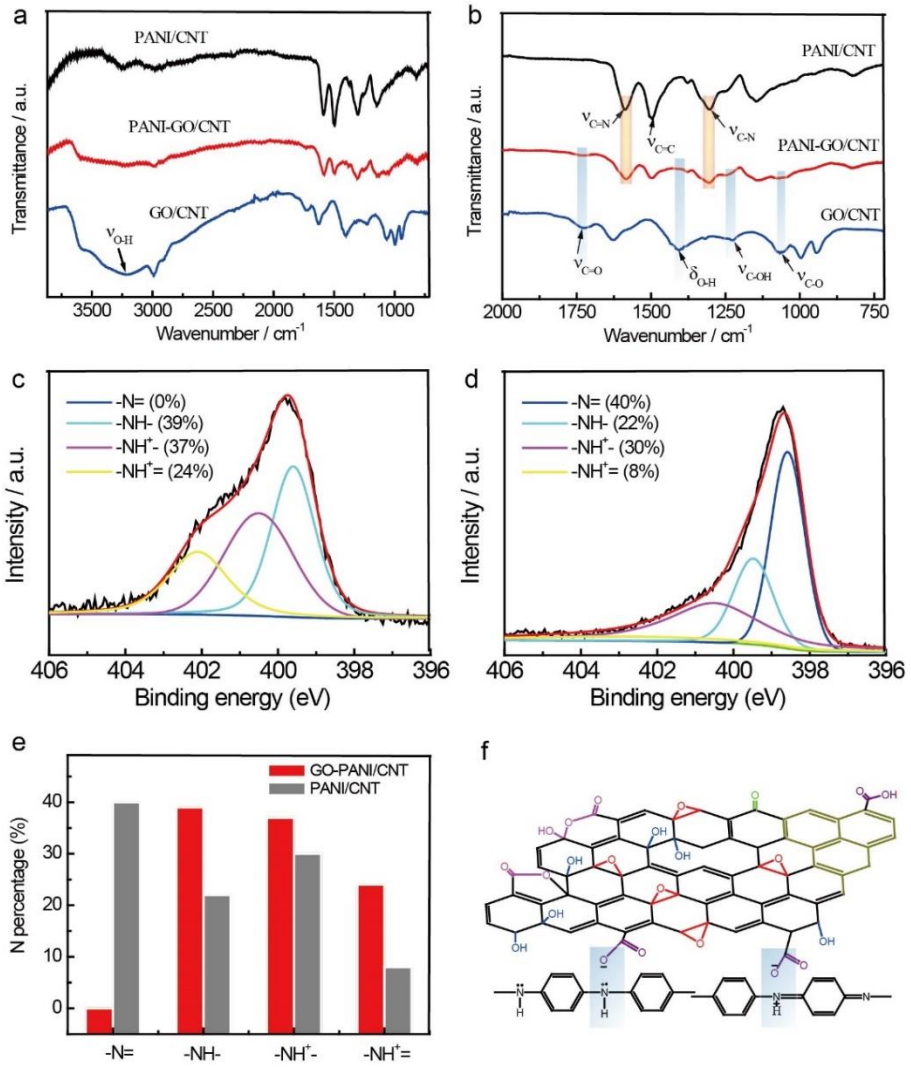

Figure 2. (a) FT-IR spectra of as-prepared PANI-GO/CNT、PANI/CNT、GO/CNT, and (b) corresponding detailed FT-IR spectra between 2000–700 cm^{-1} of the three samples.

(c)XPS N1s fits of GO doped PANI and (d) pure PANI. (e) the calculated N contents with different chemical states in GO-PANI/CNT and PANI/CNT. (f) scheme of the GO doping PANI.

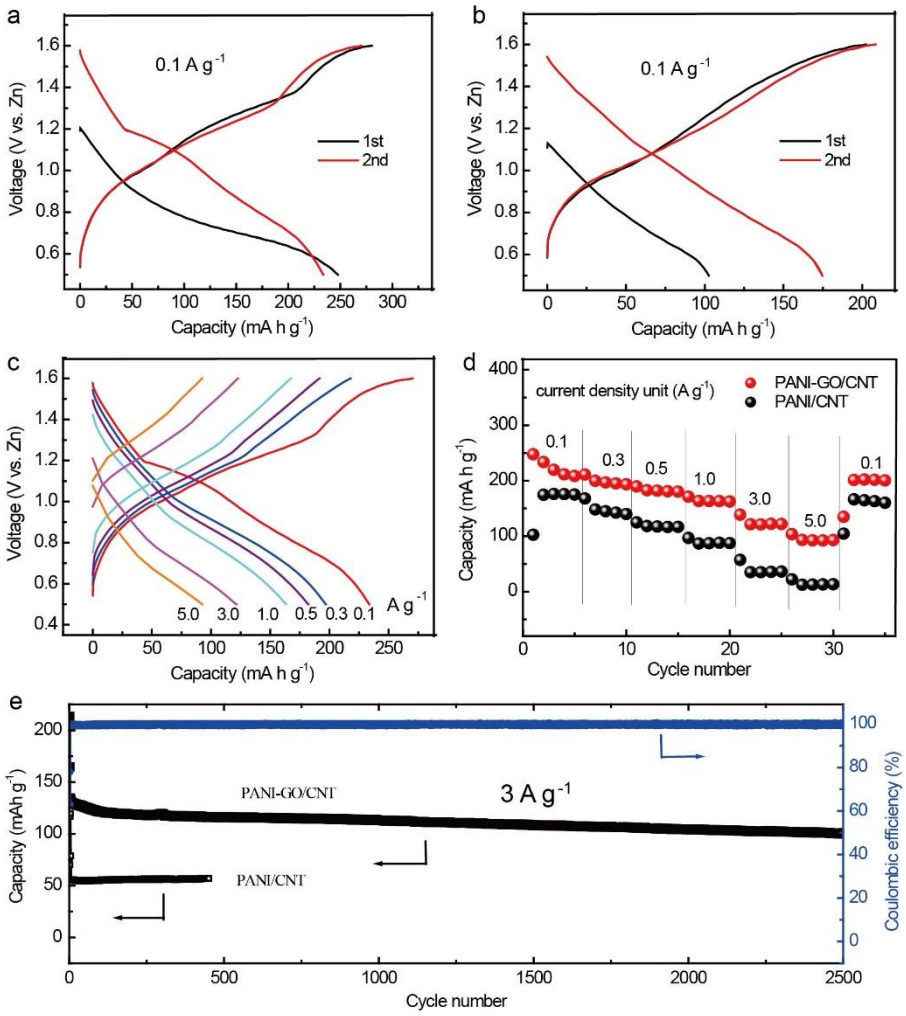

Figure 3. Galvanostatic discharge/charge voltage profiles of (a) PANI-GO/CNT and (b) PANI/CNT tested under 0.1 A g^{-1}. (c) Charge/discharge curves of PANI-GO/CNT at different current densities from 0.1 to 5.0 A g^{-1} and (d) corresponding rate performance compared with pure PANI/CNT case. (e) capacity and Coulombic efficiency during cycling at the current density of 3 A g^{-1}.

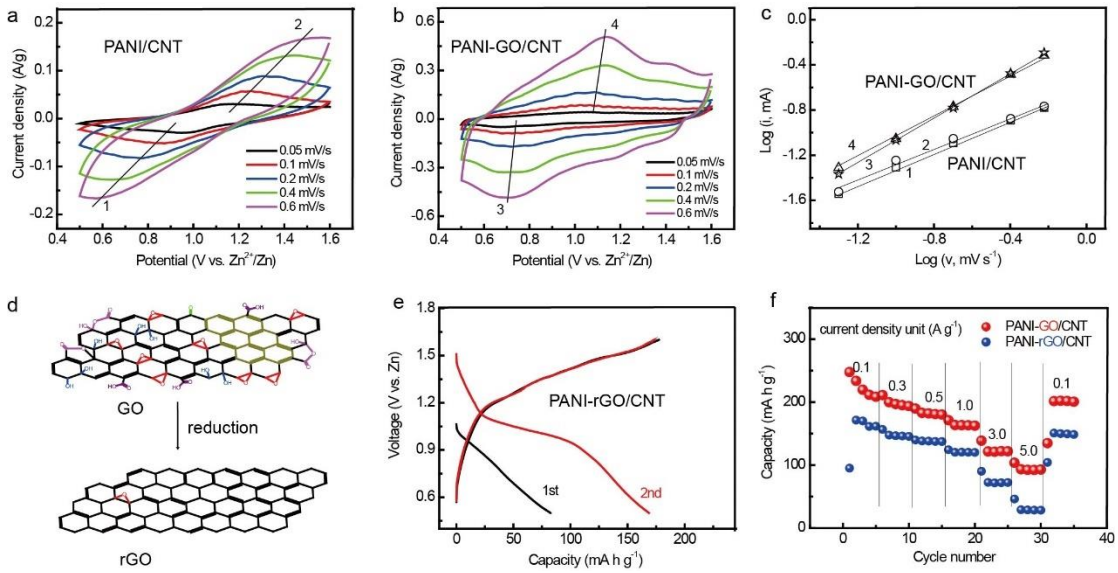

Figure 4. CV curves of (a) PANI/CNT and (b) PANI-GO/CNT at different scanning rates from 0.05 to 0.6 mV/s. (c) Determination of b values using the relationship between peak current and scanning rate. (d) scheme of removing oxygen functional groups of GO by reduction to get rGO. (e) Typical galvanostatic discharge/charge voltage profiles of reduced GO (rGO) composited PANI (denoted as PANI-rGO/CNT) and (f) corresponding rate performance compared with PANI-GO/CNT case.

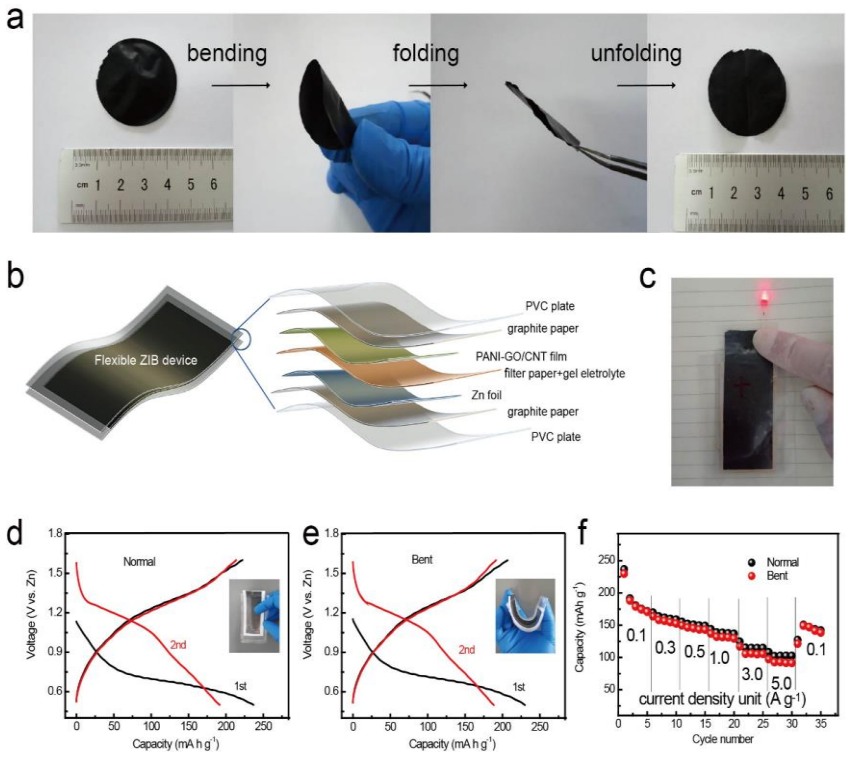

Figure 5. (a) Good flexibility of the as-obtained PANI-GO/CNT film. (b) Schematic diagram of flexible cell configuration and (c) the corresponding digital images of the flexible ZIB devices which can light up a light-emitting diode. (d) Galvanostatic discharge/charge voltage profiles of the flexible ZIB device under normal and bending state, and (f) corresponding rate performances.

Table 1. Summary of various carbon materials composited PANI cathode materials for ZIBs

PANI/carbon material composite	Specific capacity (mA h g^{-1})	Ref.
PANI/Graphene	**154** (0.1 A g^{-1}) **106** (5 A g^{-1})	25
PANI/CNT	<**160** (C/2) **70** (12 C)	26
PANI/Carbon fiber	**165** (1 C) **31** (600 C)	21
PANI/Carbon felt	**200** (0.05 A g^{-1}) **95** (5 A g^{-1})	23
PANI-GO/CNT	**233** (0.1 A g^{-1}) **100** (5 A g^{-1})	This work